JOURNAL OF MATERIALS RESEARCH AND TECHNOLOGY 2023;24:3759–3771

Available online at www.sciencedirect.com

jmr&t Journal of Materials Research and Technology

journal homepage: www.elsevier.com/locate/jmrt

Original Article

Tailoring metallurgical and biological characteristics of Ti–6Al–4V alloy by synergetic application of Nd:YAG laser and drug-loaded electrospun PVA

Tahmine Rajabi [a], *Homam Naffakh-Moosavy* [a,*], *Fatemeh Bagheri* [b], *Seyed Khatiboleslam Sadrnezhaad* [c], *Hossein Mahtab Pour* [c]

[a] *Department of Materials Engineering, Tarbiat Modares University (TMU), PO Box 14115-143, Tehran, Iran*
[b] *Biotechnology Department, Faculty of Chemical Engineering, Tarbiat Modares University, Tehran, Iran*
[c] *Department of Materials Science and Engineering, Sharif University of Technology, Tehran, Iran*

ARTICLE INFO

Article history:
Received 30 January 2023
Accepted 6 April 2023
Available online 11 April 2023

Keywords:
Ti–6Al–4V alloy
Surface modification
Nd-YAG laser
Electrospinning
Polyvinyl alcohol
Biocompatibility

ABSTRACT

Titanium alloys have been used extensively as implants. However, they generally suffer from low biocompatibility as well as antibacterial activity. To date, several strategies have been proposed to address these issues. It is of practical interest to synergistically increase both cellular adhesion and antimicrobial activity in titanium-based implants. Here, Ti–6Al–4V alloys were surface-modified by Nd:YAG laser with different scanning speeds ranging from 1 to 5 mm s^{-1} and subsequently coated by drug-loaded polymer nanofibers for prolonged drug release. The laser-modified samples were both physically and metallurgically characterized through XRD, OM, AFM, FESEM, hardness, and wettability tests to find the optimum laser processing conditions. Results showed that the surface characteristics of the alloys are sensitive to the scanning speed; the higher the scan velocity, the lower surface roughness and wettability were obtained. The enhanced formation of TiO and Ti_6O oxides on the surfaces of laser-modified alloys was delineated. Then, a model polymer/drug system of polyvinyl alcohol/vancomycin was directly electrospun onto the optimized samples surfaces. The laser-modified, drug-loaded samples present an improved biocompatibility as the cellular adhesion and viability were increased in contact with these samples. Up to 39% increase in cell viability was obtained for the laser-modified samples by 5 mm s^{-1} scan speed in comparison with unmodified, uncoated samples. The increased biocompatibility was attributed to the formation of oxide layers which reduce the toxicity of vanadium and aluminum elements. Also, the drug release rate was extended from 4 h to 25 h for modified samples. So, the modified implants could present a sustained release of antibiotics as well.

* Corresponding author.
E-mail address: h.naffakh-moosavy@modares.ac.ir (H. Naffakh-Moosavy).

https://doi.org/10.1016/j.jmrt.2023.04.044

1. Introduction

Orthopedic implant materials, especially in load-bearing applications, must be non-toxic, have excellent biocompatibility, high corrosion resistance in the body environment, an optimal combination of high strength and modulus close to the bone, high ductility, fatigue, and wear resistance [1]. Nowadays, titanium-based alloys are considered due to high corrosion resistance, high mechanical strength, wear resistance, biocompatibility properties, and bioactive surfaces, leading to better and faster integration [2].

The stability or failure of bone implants depends on a combination of biological and mechanical factors related to the implant surface and the body environment interaction [3]. The most important properties achieved through surface modification are better corrosion resistance, improved wear resistance, better integration rate, and high biocompatibility [4]. Recent studies have shown that topography and micro/nano surface characteristics can influence cell behavior [5].

Cell adhesion is one of the first steps for their growth and proliferation to create bone tissue. Studies have shown that surface chemistry and roughness depend on cell adhesion, growth and proliferation. Rough surfaces encourage the entrapment of fibrin protein, adhesion of bone cells, and mechanical stability of implants in the host bone [6]. The interaction of proteins and their receptors induces a signal that affects cell growth. Studies have shown that the adhesion and growth of MG63 cells are affected by surface roughness [7]. The adsorption of biomolecules on the surface is a dynamic process controlled by the physicochemical interaction between the surface and macromolecules. Surface energy, assessed by wettability, is a substantial quantity that is strongly related to biological interaction [8].

Implants-associated infections are caused by biofilm formation on the implant's surface. Even if infected implants are successfully removed surgically [9]. The adhesion of bacteria on the surface of titanium alloy implants is done in two steps, leading to biofilm formation on the surface. The first stage is the rapid and initial interaction between the surface of bacterial cells and the surface of the biological material. The irreversible second stage, includes specific and non-specific interactions between the proteins of the bacterial surface structures and binding molecules on the material's surface [10]. The best way to prevent biofilm formation is antimicrobial surfaces that prevent the spread of pathogens and the degradation of materials. Implants surface modification is an effective way to reduce implant infections, which is a direct method to modify the surface properties of medical implants without changing the bulk properties of the material. Surface treatment can be divided into two categories: surface modification (physical, chemical, or both) and coating (physical, chemical, or both) [10]. These techniques can be used individually or in combination. The researcher used micromachining, polishing, sandblasting, surface coating, acid etching, photolithography and laser for surface modification [3,11]. It is possible to improve the mechanical properties of the alloy, including hardness, corrosion resistance, and biocompatibility, by changing the surface properties without changing the bulk properties of the alloy using laser surface modification. The surface microstructure depends on the cooling rate during solidification and solid phase transformation, and the thickness and chemical composition of the modified zone are affected by the thermal cycle [12]. Compared to other surface modification methods, this method has advantages such as high speed, controllability, ease in complex geometries, and simplicity in reaching the desired surface chemical composition [4]. Depending on the process parameters, it may include microstructure modification, grain modification, phase transformation, alloying, combining multiple materials, and combining and forming composite systems on the surface without affecting the bulk of the material [13].

The current strategy to control infections from orthopedic implants is the periodic administration of antibiotics. Although antibiotics can be part of clinical treatment, high drug concentrations may not be achieved at the intended site. Antibiotic administration can lead to various toxicities or the development of antibiotic-resistant microorganisms. Therefore, the strategy of controlled release of antibiotics with high concentration and long duration to target the desired site and release the drug can be a promising alternative to antibiotic administration [14]. Hence, researchers have recommended the controlled release of antibiotics. Gentamicin, vancomycin, cefazolin, propylparaben, ceftizoxime, and lysostaphin are antibiotics used to treat orthopedic infections [15]. Biodegradable polymer-coated implants can deliver antibiotics to the site [9]. A relatively novel and versatile method to apply an antibacterial coating to the implants surfaces is electrospinning. By this technique, nanofibers carrying an antibiotic drug are directly deposited onto the surface of the implants to a desirable content. The whole process does not require any pretreatment. However, the microstructure of the coating as well as their biological properties such as drug release rate can be tuned by controlling the fabrication parameters or by some subsequent treatments [16]. To date, various bio-based or biodegradable polymers were fabricated via electropsinning, among which polyvinyl alcohol (PVA) has attracted increasing attention due to its extremely good spinnability, biocompatibility, hydrophilicity, and drug delivery potentials [17].

In 2020, Tullio et al. [18] presented in vivo studies of titanium implantation with three machined, sandblasted/acid etched, and laser-modified surfaces. The results showed that after 30 days, the laser-modified samples and the sandblasted/acidified sample showed greater integrity than the machined sample. In 2021, researchers investigated the effect of groove spacing and micromachining laser frequency on surface modification and biological properties of Ti–6Al–4V alloy. The results showed that the depth of the laser layer was reduced by increasing the groove distance and frequency, improving the survival results of cell adhesion in laser-modified samples [19].

In this research, Nd:YAG laser was used for surface modification of Ti–6Al–4V alloy. The electrospinning process of biodegradable polyvinyl alcohol polymer carrying vancomycin was used on the modified-surfaces for drug delivery.

Table 1 – Nd:YAG laser parameters for sample preparation.

Sample group	Sample group name	Laser scanning speed (mm/s)	Frequency (Hz)	Voltage (V)	Power (W)	Gas flow (L/min)
1	N1	1	10	400	100	20
2	N3	3				
3	N5	5				

2. Materials and methods

2.1. Surface modification

Firstly 50 × 15 mm specimens were cut from a 1 mm thick Ti–6Al–4V sheet (90.7% Ti, 5.6% Al, 3.5% V, 0.2 Fe). Then samples were ground and polished to remove any oxides and contaminations and achieve a smooth surface. Finally, samples were sonicated in ethanol and DI water solution. A 100 W Nd: YAG pulse laser performs laser surface modification of samples. According to choosing three laser scanning speeds, as mentioned in Table 1, three groups of samples containing three samples were modified in this process. The position of samples on the instrument's table is adjusted by its lens. During the experiment, the laser beam was fixed, and surface scanning of the samples was done by moving the table along x and y directions.

2.2. Drug-loaded surface coating

Solution 1, PVA: 12 wt% polyvinyl alcohol (86–90% hydrolyzed, MW 105–110 D) solution was prepared in distilled water. The Solution was stirred for 3 h under a continuously growing temperature until 80 °C. Solution 2, vancomycin: 2.4 wt% vancomycin solution was prepared by dissolving vancomycin powder in distilled water under continuous stirring for 30 min at ambient temperature. Solution 3, drug-loaded PVA: 8 wt% PVA, 0.8 wt% vancomycin solution prepared using solutions 1 and 2 with a ratio of 2: 1 and stirred for 30 min. Fig. 1 investigates the electrospinning process on the surface of laser-modified samples.

Laser surface modified specimens were cleaned ultrasonically using DI water for 10 min and then dried. Specimens were fixed on an aluminum foil, and all parts of the foil except the samples were insulated. Electrospinning was carried out for 2 h at ambient temperature. Feed rate 0.1 ml/min, voltage 15 kV, and distance 15 cm were applied to electrospinning. Laser surface-modified Specimens coated by drug-loaded electrospun fibers were dried at ambient temperature for 24 h. The fibers were chemically stabilized through vapor-phase glutaraldehyde crosslinking. A solution of 0.5 wt% glutaraldehyde in acidified ethanol was placed in a closed container and the samples' coated surface were exposed to the vapor for 3 days. After completing of the cross-linking process, specimens were washed using ethanol and dried.

2.3. Metallurgical characterization

In contact mode, the roughness topography and profiles in laser surface-modified samples were investigated by Atomic Force Microscopy (AFM, Veeco CPII model). Optical Microscopy (OM, Dinolite type) was used to assess the surface wettability according to ASTM D7490-13 standard by taking pictures of contact angles. Field Emission Scanning Electron Microscopy (FE-SEM, MIRA III model) at 10 kV, equipped with an Energy Dispersive X-Ray Spectroscopy (EDS, SAMX model) and Optical Microscopy (OM, Leica model) were used for surface and cross-sectional microstructure evaluation. The hardness of surface modified samples cross-section was measured using Vickers Microhardness Tester (Buehler model) using 10 gf load according to the ASTM E384-17 standard. Such measurements are repeated at least three times and the hardness of each zone is determined as the average of three measurements. X-ray Diffraction Test was performed according to BS EN 13925–1 at 40 V, 30A (XRD, model PW1730), and surface composition was extracted from Expert Highscore software.

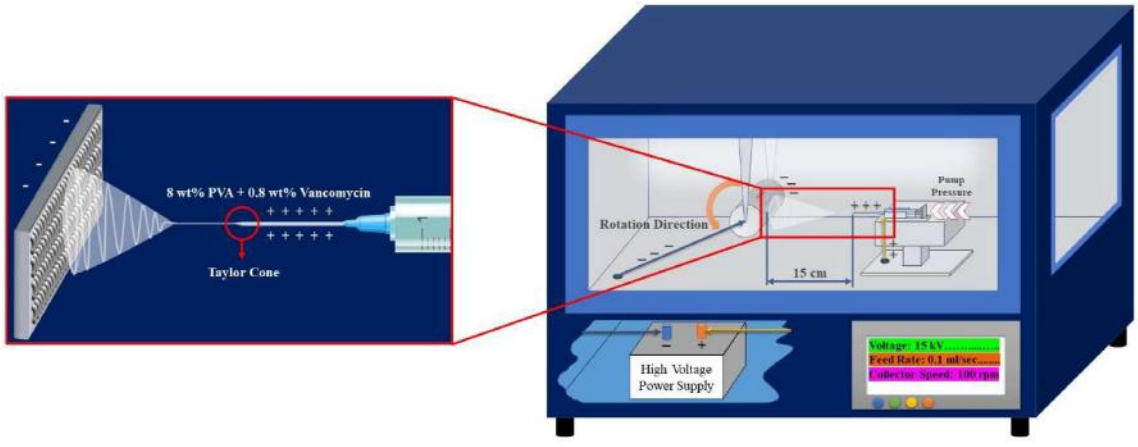

Fig. 1 – Laser modified samples electrospinning process schematic.

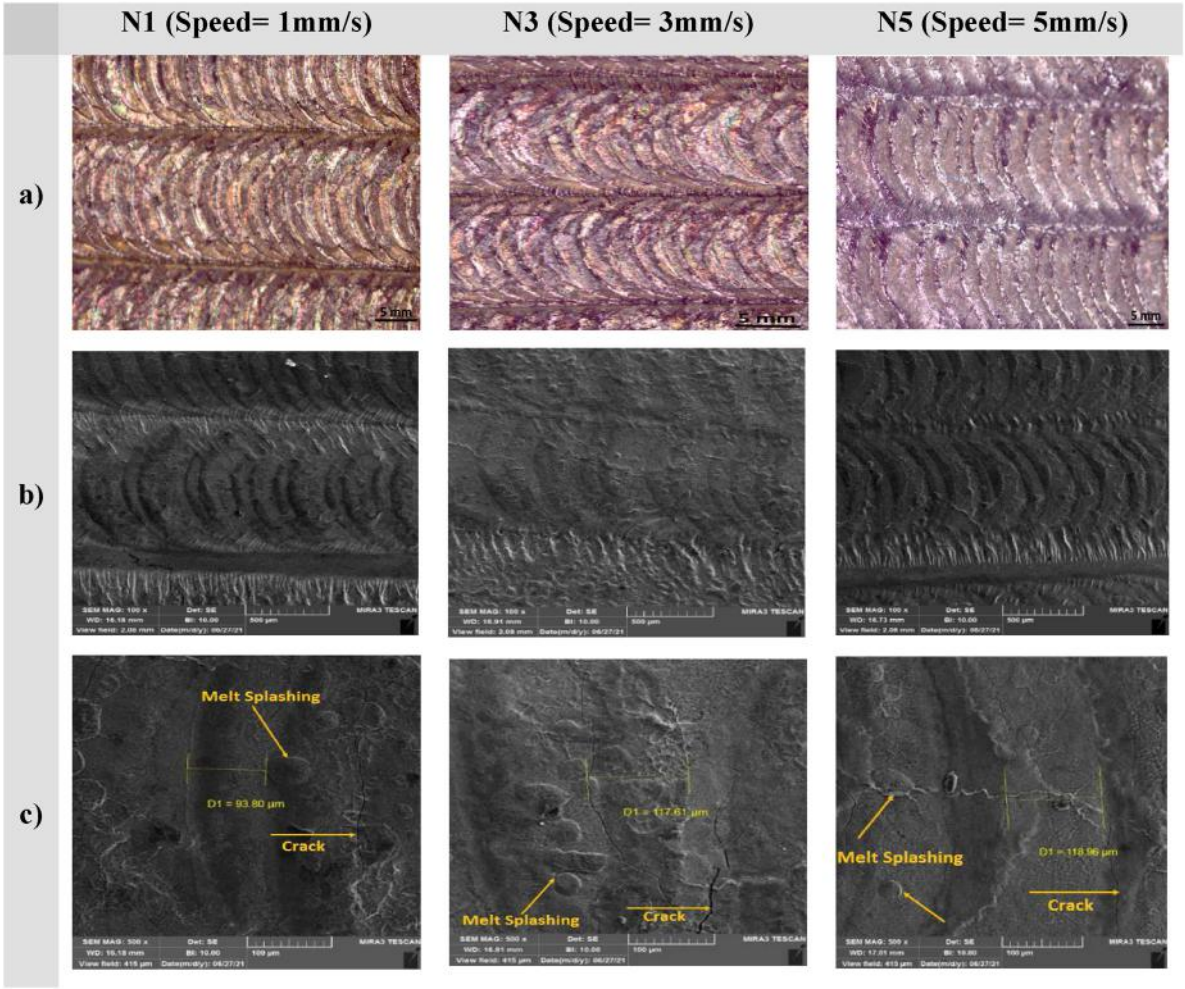

Fig. 2 – (a) Weld beads optical micrograms (b) SEM images of columnar microstructure of the weld zone normal to the weld line (c) SEM images of microcracks propagation perpendicular to the weld line.

2.4. *Coating characterization*

Morphology and distribution of electrospun polyvinyl alcohol fibers were characterized using Field Emission Scanning Electron Microscopy (FE-SEM, MIRA III model) after electrospinning and after the crosslinking process.

2.5. *In- vitro biological evaluation*

In order to perform in vitro cellular evaluation, MG-63 human osteoblast-like cell was used. For cell culture on the laser surface modified and coated samples, the samples were first sterilized using 70% alcohol. Then 30,000 cells were cultured on each sample (1.5 × 1 cm).

2.5.1. *Cell viability*

MTT test was used to asses cell viability on the fourth day. The culture medium on the samples was removed and replaced with MTT solution (5 mg/ml) diluted with the medium. The samples were incubated in a CO_2 incubator for 4 h. Then the solution was removed from the samples. DMSO was poured into each well to dissolve the formed purple formazan crystals and gently pipetted to dissolve the formed crystals completely. Then the resulting solution was transferred to a 96-well plate. The optical absorbance of the solution was read at a wavelength of 545 nm using a microplate reader. This test was repeated three times for each sample using a microplate reader, and the result's average value and standard deviation were calculated.

2.5.2. *Cell adhesion assay*

After 4 days of cell culture, the samples were fixed using 2.5% glutaraldehyde for 1 h. Then the samples were dehydrated with an increasing percentage of ethanol and dried at ambient temperature. Then the samples were coated with gold and photographed with a scanning electron microscope.

2.5.3. *Drug release*

UV–Vis spectrometer was used to evaluate vancomycin release from the coated fibers on the sample's surface. First, the absorption curve of vancomycin in concentrations of 0.05, 0.1, 0.15, 0.2, and 0.25 mg/ml was drawn at a wavelength of 282 nm, and the absorption equation was obtained. Then the measurement of drug release in Nd:YAG laser surface modified at a speed of 1 mm/s samples and the samples without surface modification was done as follows:

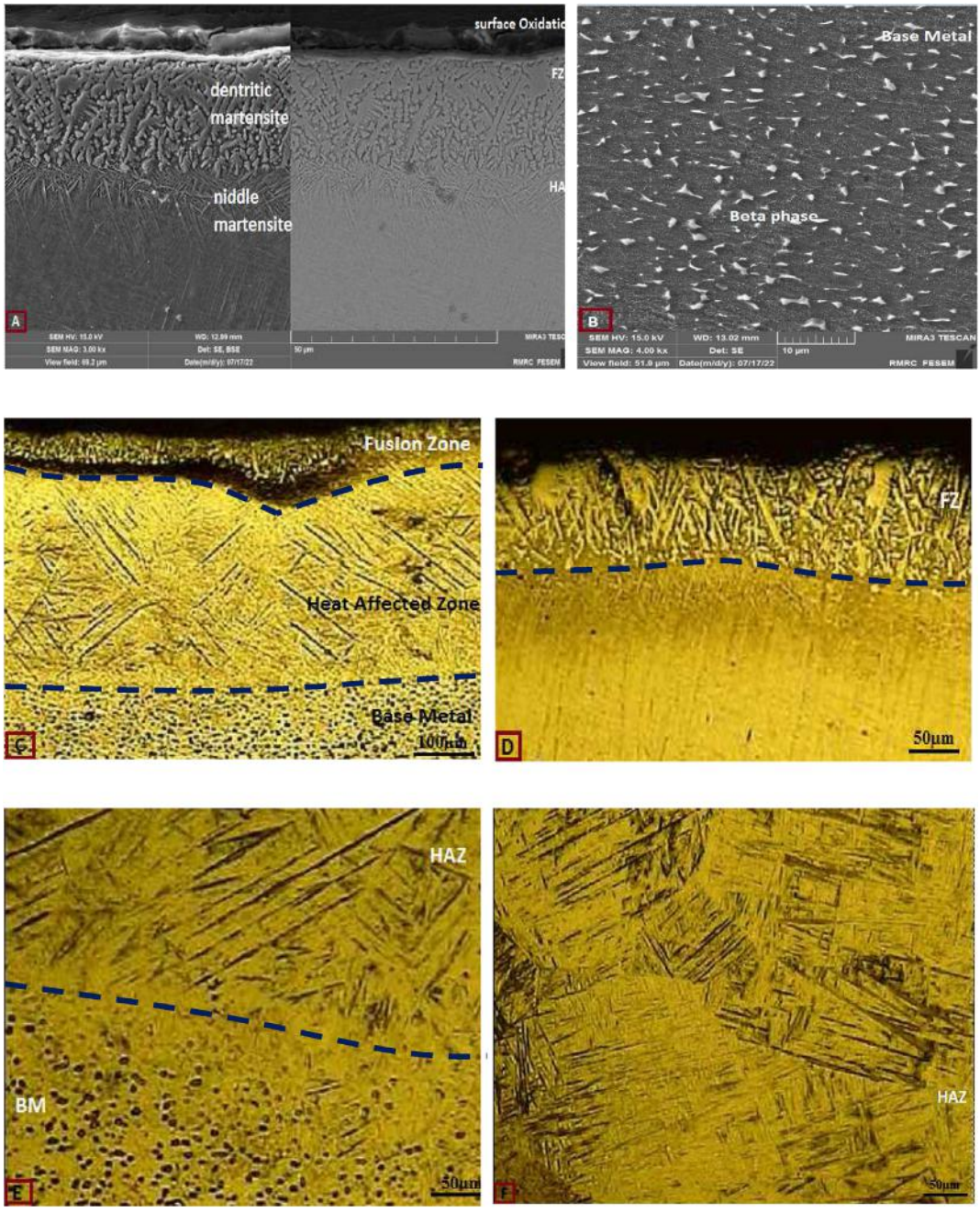

Fig. 3 – (a) Cross-sectional SEM image of laser treated sample left side: dendritic and needle martensite microstructure right side: formation of passive surface oxide layer (b) SEM image of sample's phase structure (c–f) Cross-sectional optical micrograms of weld zones.

The samples were immersed in 4 ml buffer solution at 37 °C and 75 r/min. Then, after the specified time, 2 ml was removed from the solution, and its absorption rate was measured to calculate the percentage of the released drug. Then 2 ml of buffer solution was added to the release medium. This process was done at 1, 2, 4, 6, 15, 25, 30, 50, and 60 h. The concentration of the released drug was obtained using the absorption equation and absorption values according to Eqs. (1) and (2).

$$R\% = \frac{M_i}{M_t} \times 100 \quad (1)$$

$$M_i = C_i V_i + \sum C_{i-1} V_i \quad (2)$$

where R, M_i, M_t, C_i, V_i, and C_{i-1} represent the accumulation percent of the released drug, released drug at time 0-t, total loaded drug on the sample surface, concentration at time t,

volume of removed solution, the concentration at the time before t, respectively.

2.6. Statistical study

Statistical analysis was carried out by using a statgraphics statistical software package. The quantitative results were presented as the means ± SE for each group.

3. Results and discussion

3.1. Scanning pattern on the surface of laser modified samples

Fig. 2a shows the optical microscopy pictures of Nd:YAG laser-modified surfaces. The distance between laser beads (D) can be calculated by laser scanning speed (S) and laser pulse frequency (F) ratio as determined by Eq. (3) [20]. At constant laser frequency, laser beads distance increases as laser scanning speed increases because the number of pulses per unit area and the interaction between laser pulses and sample surface decreases, and less energy is transferred to the surface. Therefore, as laser scanning speed increases, the distance between peaks and valleys increases and decreases surface roughness [21].

$$D = \frac{S}{F} \tag{3}$$

Scanning electron microscopy images in Fig. 2b and c shows welding beads. Along the weld line, the columnar microstructure of the weld zone, which is normal to the weld line, can obviously be seen and confirms directional solidification. Several microcracks can be seen mostly along the solidification direction and perpendicular to the welding line. These cracks can be seen as the result of tensile forces after Shrinkage caused by melt solidification. According to Rosenthal's equation, Eq. (4) can be deduced. Eq. (4) shows that in constant heat Q, increasing the laser speed increases the cooling rate. Because of higher residual stress caused by a higher cooling rate, samples modified with a speed of 5 mm/s have a higher probability of hot cracking.

$$\left(\frac{\partial T}{\partial t}\right) = \left(\frac{\partial T}{\partial x}\right)_t \left(\frac{\partial x}{\partial t}\right)_T = -2\pi KV\,\frac{(T - T_0)^2}{Q} \tag{4}$$

where T, T_0, K, Q, and V represent temperature at time t, temperature before welding, heat conductivity, heat transferred to the specimen, and speed, respectively.

In addition, increasing the laser speed increases the solidification growth rate and decreases the temperature gradient. The temperature gradient affects the length of the solidification crack sensitive zone (CSZ) and increases with increasing speed. As the speed and the length of the CSZ zone increase, permeability decreases due to the formation of narrower and longer interdendritic liquid channels, making it more difficult to feed contractions caused by solidification. Inconsistent physical properties of the oxide layer and substrate lead to the ununiform distribution of tensions between two layers during solidification and may lead to surface cracks [22]. Also, in all the modified samples, melt splashing occurred due to the high heat density caused by laser welding and the melt pool's high pressure and temperature.

3.2. Microstructure and microhardness of samples cross-section

The cross-sectional FE-SEM image of Fig. 3 shows a dark layer of titanium oxide formed on the surface modified at a laser speed of 3 mm/s. The formation of the passive oxide layer affects the potential, rate, temperature, and electrolyte of corrosion. Therefore, the biocompatibility of titanium alloys depends on the interaction between the titanium oxide layer's physicochemical, morphological, and mechanical properties [23]. Cross-section optical microscopy images reveal a dendritic structure is obtained in the melting zone, and a martensitic structure is obtained in the heat-affected zone close to the melting zone. The base metal also contains the β phase in a background of the α phase. Argon gas atmosphere causes the decrease of temperature of the solid/melt interface during its advance into the melt. During solidification, heat is removed from the melt and the solid, and latent heat release at the solid/melt interface makes it unstable due to its upper temperature than solid and melt. The unstable interface leads to surface roughness and can become dendritic branches that grow from the interface toward the melt. The high cooling rate in the heat-affected zone results transformation of the β-phase to martensitic microstructure. At the boundary of the heat-affected zone/base metal, β phase dissolved due to the high temperature and created the supersaturated α-phase.

Variation of microstructural characteristics induced by pulsed laser treatment can increase hardness [24]. Laser surface treatment of Ti–6Al–4V sheets can increase the hardness by solid solution of alloying elements, grain refinement and nanotwins mechanisms [25,26]. The α-phase has lower hardness and higher ductility than the β-phase. Martensite α'-phase has higher hardness than both α and β phases [27]. Cross-section microhardness results of the modified sample in Table 2, indicate the presence of titanium oxide on the surface due to higher hardness. In the fusion zone, the presence of dendritic structure has caused higher hardness. Moving away from the fusion zone, the hardness is still high due to needle martensite in the heat-affected zone. The hardness is lower than the fusion and heat-affected zones in the base metal, where there is a higher percentage of α-phase. The high hardness values of the dendritic martensite phase in the fusion zone and needle martensite in the heat-affected zone improve the wear properties and more resistance to galvanic corrosion compared to the α+β microstructure, because of the existence of the two layers and the creation of galvanic interaction between the two phases.

Table 2 – Cross-sectional Vickers microhardness results of laser modified specimens.

Zone	Vickers Microhardness
Surface	1275
Fusion Zone	408
Heat Affected Zone	362
Base Metal	334

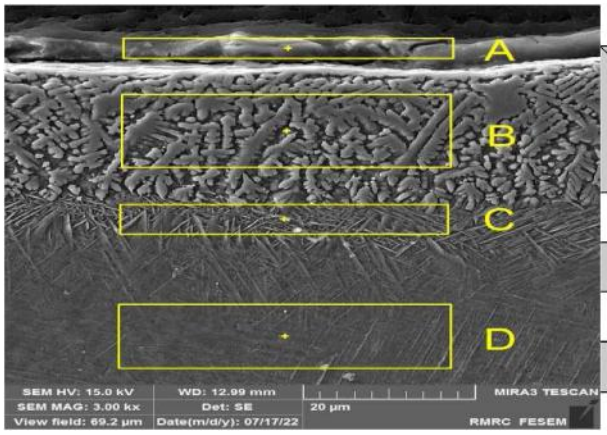

Zone / Element	A	B	C	D
Ti (%wt)	16.4	93.3	91.2	90.8
Al (%wt)	22.98	5.2	7	6.9
V (%wt)	0	1.5	1.8	2.3
O (%wt)	60.7	0	0	0

Fig. 4 – Chemical composition of laser treated sample (3 mm/s) in weld zones and base metal.

3.3. *Compositional analysis of modified samples cross section*

Fig. 4 investigates the structure and chemical composition of Ti–6Al–4V implants modified at the speed of 3 mm/s. EDS results in surface area (A), fusion zone (B), heat affected zone (C), and heat affected zone near the base metal (D) investigated. The presence of 60.68% weight of oxygen on the surface confirmed the formation of the surface oxide layer. The presence of high amounts of aluminum in the surface layer results from the high tendency of this element to oxidize. The percentage of Al and V elements in the fusion zone was lower than in the heat-affected zone close to the base metal (D), and by moving from the fusion zone to the base metal, the values of these elements increased. Due to the high temperature of the laser process, it is possible that these elements have evaporated. Also, due to aluminum high tendency to oxidation and the increase in the amount of this element in the surface oxide layer, the decrease in the amount of this element in the melting zone can be attributed to surface oxidation. Aluminum and vanadium elements are toxic, and reducing their amounts in the surface layer can improve biological properties. Also, there is no concern about the effect of these elements' reduction on the alloy's properties because of the small effect depth of the laser in the cross-section.

3.4. *Surface modified samples phases*

X-ray diffraction pattern of laser-modified sample surfaces in Fig. 5 shows the existence of three phases. Ti_6O, as Ti-rich titanium oxide, forms when oxygen diffuses into the hexagonal primary lattice of α-Ti. The formation of the cubic TiO phase is due to the stabilization of cubic β-Ti during rapid solidification and α-Ti phase symmetric growth [28].

Due to the high speed of the laser surface modification and insufficient time to form TiO_2, the combined oxygen ratio was equal to 1:12 for Ti_6O and 1:2 for TiO in the conventional state. The formation of the titanium oxide layer improves the implant surface osseointegration, adhesion properties, corrosion and wear resistance. Increasing the thickness of the oxide layer, even by a picometer, leads to exponential improvement of biological properties.

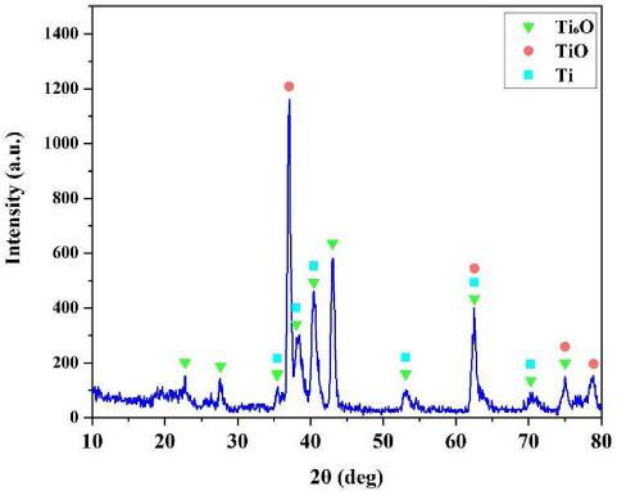

Fig. 5 – X-ray diffraction pattern of laser modified samples surface.

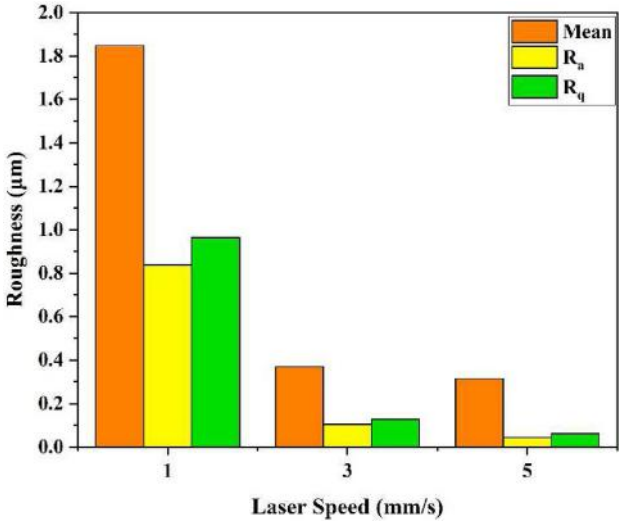

Fig. 6 – Effect of laser speed on surface roughness parameters of sample surface.

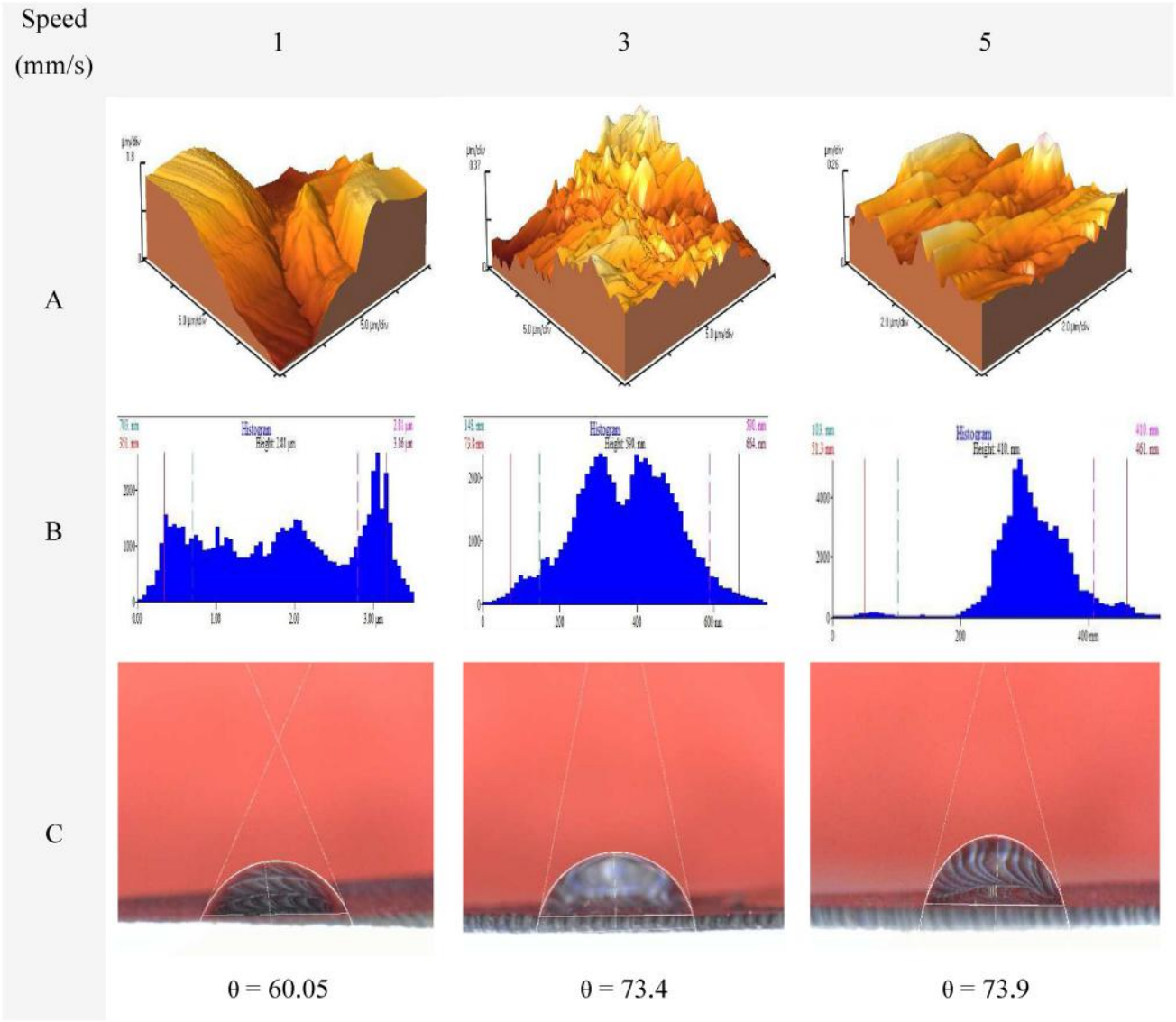

Fig. 7. – (a) surface topography (b) surface roughness profile and (c) Effect of surface roughness on the surface wettability of laser modified samples.

3.5. *Surface topography as a function of Nd: YAG laser speed*

Figs. 6, 7a and 7b show the surface roughness parameters, topographies, and profiles of surface-modified specimens. As shown, increasing laser scanning speed results in decreasing roughness parameters such as the mean of roughness from 1.85 to 0.03 μm and height of roughness from 0.8 to 0.04 μm and the highest surface roughness values are related to the surface-modified specimens with the lowest speed.

At high laser speeds, the laser beam has a shorter time interacting with the surface, and the energy absorbed by the surface is less, reducing the roughness parameters. Therefore, rougher surfaces are obtained at lower laser speeds [9]. The relationship between the accumulation energy and the laser parameters can be expressed according to Eq. (5):

$$F = \frac{Ep.f}{D.V} \quad (5)$$

In the above relation, F, Ep, f, D, and V represent the accumulation energy, pulse energy, frequency, laser spot diameter, and velocity, respectively. This relationship indicates the inverse relationship between the amount of energy absorbed and the velocity of the laser beam [29].

3.6. *Wettability as a function of Nd:YAG laser speed*

The effect of Nd: YAG laser speed on the wettability of the modified surfaces is shown in Fig. 7c. According to Fig. 7c, the contact angle changes from 60.05° to 73.9° with the alteration of laser scanning speed from 1 to 5 mm/s. Since the highest roughness was related to the sample with the lowest laser speed, the lowest contact angle of the droplet with the surface,

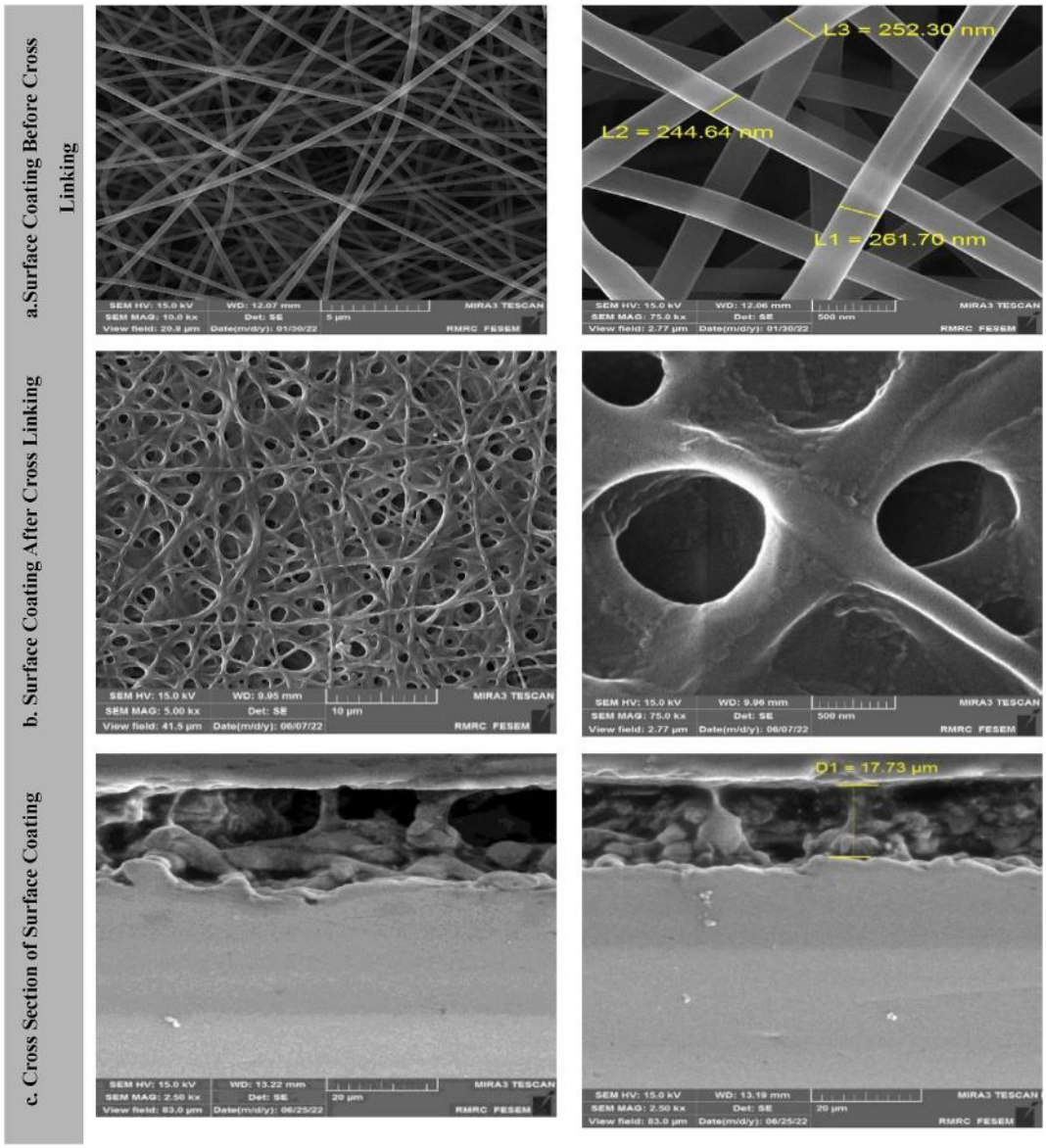

Fig. 8 – SEM images of (a) PVA electrospun fibers on the surface of laser modified samples (b) Cross-linked PVA fibers (c) Cross-section of coating thickness.

and the highest wettability was related to the sample with a speed of 1 mm/s. The Young equation and the relation between roughness and contact angle describe the reason for this observation. Young equation (Eq. (6)) determines the equilibrium between the solid, liquid, and gas phases interface.

$$\gamma_{LV} \cos\theta = \gamma_{SV} - \gamma_{SL} \quad (6)$$

where γ_{LV}, γ_{SV}, and γ_{SL} are surface tension between liquid-solid, solid-vapor, and solid-liquid phases interface, respectively, and θ is the contact angle. When a liquid is in contact with a solid surface, contact angle and surface tension are related to each other with the Young equation. If $\theta < 90$, the solid surface wet well with liquid [30]. Hideo et al. suggested the relation between wettability and surface roughness of a solid surface by Eq. (7).

$$\cos\Phi = (h/(h+R))\cos\theta - R/(h+R) \quad (7)$$

In this equation, Φ is the observed contact angle, θ is the contact angle, h is the roughness height, and R is the droplet radius [31]. According to this relation, wettability decreases with the increment of scanning speed due to roughness height decrease.

According to the Wenzel model, droplet wettability on rough surfaces is expressed as Eq. (8).

$$\text{Cos}\ (\theta_W) = \text{Rf Cos}\ (\theta_Y) \quad (8)$$

where θ_W and θ_Y represent the contact angles of Young, Wenzel, and R_f, represents the fraction of the A_{SL} liquid-solid contact surface to the predicted region on the A_F solid surface. In Wenzel's model, liquid penetrates and fills the gap between the grooves on the rough surface. On rough surfaces, given that $R_f > 1$, if Cos θ_Y is greater than zero, the liquid tends to wet the rough surface, and if Cos θ_Y is less than zero, the liquid tends not to wet the surface. The wettability properties of the

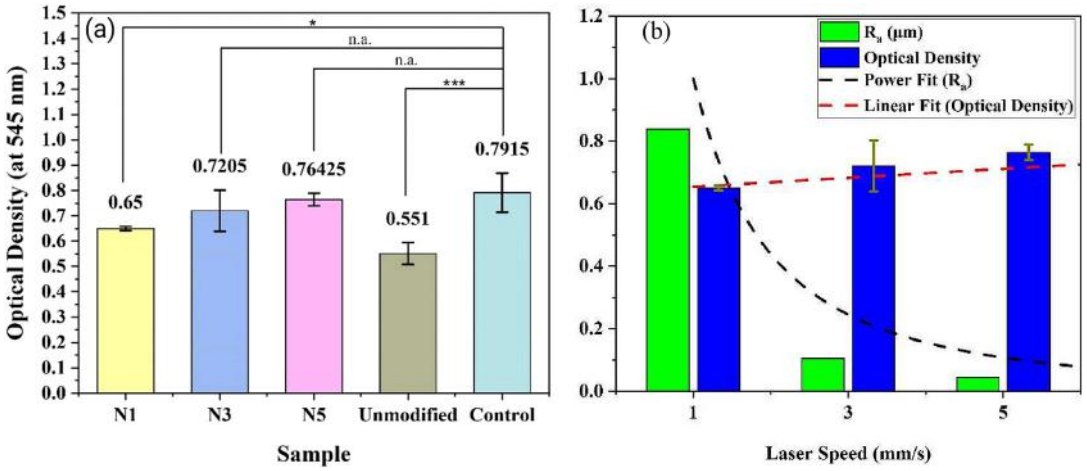

Fig. 9 – (a) Cell viability of modified samples compared to control sample (cells cultivated in the culture plate) *P <0.05, ***P<0.001 (b) effect of surface roughness on cell viability.

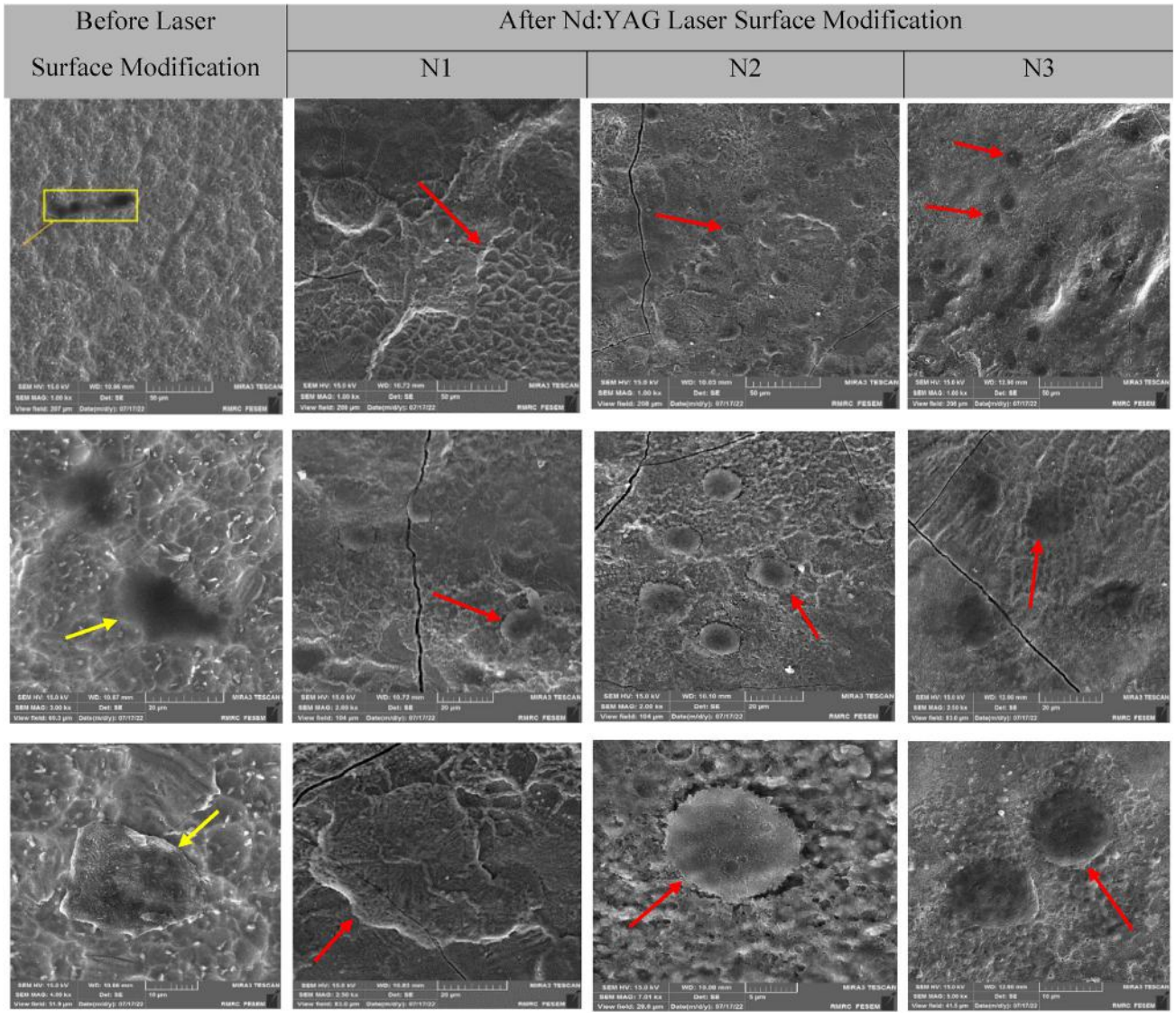

Fig. 10 – Effect of surface modification on cell adhesion.

surface depend on the roughness factor that can turn the surface into a hydrophobic or hydrophilic surface [9]. By increasing laser speed and decreasing the values of roughness parameters and R_f, the contact angle of the droplet decreased so that the sample with the highest laser speed (5 mm/s) had the lowest wettability.

3.7. Coating characterization

Vancomycin-loaded polyvinyl alcohol electrospun coating, before and after cross-linking, is given in Fig. 8a and b and shows that the average diameter of the fibers increased after cross-linking, and micron-sized holes were created in the coating. The formation of these cavities can be a place to attract osteoblast cells and leads to better interaction between the implant surface and body tissue.

Due to the surface roughness of the modified samples, the electrospun fibers have been mechanically established on the surface. The thickness of the coating in Fig. 8c, is shown. Due to the Biodegradability of polyvinyl alcohol, 75% of the coating will be destroyed after 46 days [32] and the implant's modified surface is exposed to the body tissue. Therefore, the adhesion and interaction of bone cells with the laser surface modification becomes important.

3.8. Biological analysis

3.8.1. Cell viability

Fig. 9a investigates laser-modified and coated Ti–6Al–4V alloys have higher cell survival than the sample with no surface modification and coating process, which confirms toxicity reduction as a result of Nd:YAG laser surface modification and coating. The formation of the oxide layer on the surface of the modified samples can be one of the reasons for these observations, which has increased the cell viability due to good biological properties. The lower percentage of vanadium element on the surface can be another reason for the lower toxicity of modified samples.

Cell viability has increased by incrementing the Nd:YAG laser speed. Therefore, although the increase in surface roughness has reduced cell survival and proliferation compared to the control sample, the samples with less roughness had better cell survival. The reason for this could be the high contact area of rougher samples. The relationship between surface roughness and toxicity is shown in Fig. 9b. From this point of view, the optimal roughness value of the modified samples is at a speed of 5 mm/s.

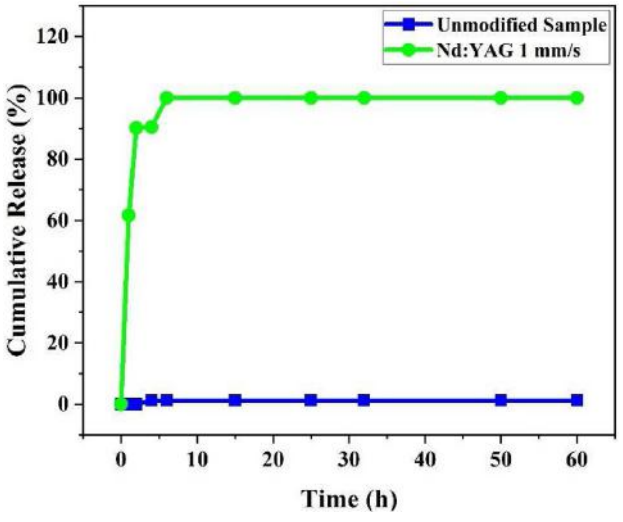

Fig. 11 – Drug release rate variation between unmodified and laser modified sample.

3.8.2. Cell adhesion

Cell adhesion on the surface of unmodified and laser surface modified samples is shown in Fig. 10. According to the MTT results, the unmodified surface has the lowest cell viability, which can be seen by low cells distribution on the surface. The adhesion and morphology of cells on the surface of Nd:YAG laser-modified samples show an increase in cell density with increasing speed, due to reduced toxicity in high-speed laser-modified samples. Cells in all modified samples have an elongated morphology and fully interact with the surface.

3.8.3. Drug release rate

The cumulative percent curve of drug release in terms of time in Fig. 11 investigates different release rates in unmodified and laser surface-modified samples. The low drug release rate in the unmodified-sample can result from lower roughness. In the laser-modified samples, a higher drug release rate was observed, so 90% of the drug was released after 2 h and 100% after 6 h. The amount of released drug in the unmodified samples was 1% of that in the laser surface-modified samples.

Nd:YAG Laser surface modification results to surface roughness and hydrophilicity increment. So, the rougher surfaces of the laser-modified samples interacted more with body fluids and showed more drug release than the non-modified surface samples.

4. Conclusion

In this research, Nd:YAG laser surface modification of Ti–6Al–4V alloy has led to an increment of surface roughness, wettability, hardness, and controlled drug release of polyvinyl alcohol fibers coating has improved biocompatibility and cell adhesion.

The results are summarized as follows.

1. The phases formed in the Nd:YAG laser surface-modified samples included dendritic martensite in the fusion zone, acicular martensite in the heat-affected zone, and the formation of TiO and Ti_6O oxides on the surface.
2. By moving from the base metal to the heat-affected and the fusion zone, the amount of aluminum and vanadium elements has decreased.
3. Due to the formation of the martensite phase, laser surface modification increased the hardness of the fusion zone and heat-affected zone without any effect on the bulk properties. The highest hardness was related to the surface oxide layer.
4. The highest wettability was related to the surfaces with the highest roughness. Therefore, the modified samples with a speed of 1 mm/s showed the highest hydrophilicity.
5. All Nd:YAG laser surface-modified samples with different speeds showed less toxicity than the sample without surface modification.

6. Cell viability has improved by laser surface modification. The surface-modified sample with a speed of 5 mm/s showed more cell viability than the other groups.
7. Surfaces with less roughness have shown less toxicity.
8. Laser surface modification has increased cell adhesion.
9. Drug release has improved in laser surface modified compared to the unmodified surface samples because of increasing electrospinning fiber attachment on the rough surface.

Declaration of competing interest

The authors declare that they have no known competing financial interests or personal relationships that could have appeared to influence the work reported in this paper.

Acknowledgement

The authors of this article express their gratitude to Dr. F. Soleimani for his valuable guidance in the field of electrospinning.

REFERENCES

[1] Geetha M, Singh AK, Asokamani R, Gogia AK. Ti based biomaterials, the ultimate choice for orthopaedic implants–a review. Prog Mater Sci 2009;54:397–425.
[2] Kirmanidou Y, Sidira M, Drosou M-E, Bennani V, Bakopoulou A, Tsouknidas A, et al. New Ti-alloys and surface modifications to improve the mechanical properties and the biological response to orthopedic and dental implants: a review. BioMed Res Int 2016;2016.
[3] Liu Q, Li W, Cao L, Wang J, Qu Y, Wang X, et al. Response of MG63 osteoblast cells to surface modification of Ti-6Al-4V implant alloy by laser interference lithography. J Bionic Eng. 2017;14:448–58.
[4] Mohammed MT, Khan ZA, Siddiquee AN. Surface modifications of titanium materials for developing corrosion behavior in human body environment: a review. Procedia Mater. Sci. 2014;6:1610–8.
[5] Hall DJ, Urban RM, Pourzal R, Turner TM, Skipor AK, Jacobs JJ. Nanoscale surface modification by anodic oxidation increased bone ingrowth and reduced fibrous tissue in the porous coating of titanium–alloy femoral hip arthroplasty implants. J Biomed Mater Res Part B Appl Biomater 2017;105:283–90.
[6] Park S-J, Bae S-B, Kim S-K, Eom T-G, Song S-I. Effect of implant surface microtopography by hydroxyapatite grit-blasting on adhesion, proliferation, and differentiation of osteoblast-like cell line, MG-63. J Korean Assoc Oral Maxillofac Surg 2011;37:214–24.
[7] Zareidoost A, Yousefpour M, Ghaseme B, Amanzadeh A. The relationship of surface roughness and cell response of chemical surface modification of titanium. J Mater Sci Mater Med 2012;23:1479–88.
[8] Rosales-Leal JI, Rodr\'\iguez-Valverde MA, Mazzaglia G, Ramón-Torregrosa PJ, D\'\iaz-Rodr\'\iguez L, Garc\'\ia-Mart\'\inez O, et al. Effect of roughness, wettability and morphology of engineered titanium surfaces on osteoblast-like cell adhesion. Colloids Surfaces A Physicochem Eng Asp. 2010;365:222–9.
[9] Pan C, Zhou Z, Yu X. Coatings as the useful drug delivery system for the prevention of implant-related infections. J Orthop Surg Res 2018;13:1–11.
[10] Adams CS, Antoci V, Harrison G, Patal P, Freeman TA, Shapiro IM, et al. Controlled release of vancomycin from thin sol-gel films on implant surfaces successfully controls osteomyelitis. J Orthop Res 2009;27:701–9.
[11] Liu Y, Rath B, Tingart M, Eschweiler J. Role of implants surface modification in osseointegration: a systematic review. J Biomed Mater Res, Part A 2020;108:470–84.
[12] Šugár P, Kováčik J, Šugárová J, Ludrovcová B. A study of laser micromachining of PM processed Ti compact for dental implants applications. Materials 2019;12:2246.
[13] Kurella A, Dahotre NB. Surface modification for bioimplants: the role of laser surface engineering. J Biomater Appl 2005;20:5–50.
[14] Zhang L, Yan J, Yin Z, Tang C, Guo Y, Li D, Wei B, Xu Y, Gu Q, Wang L. Electrospun vancomycin-loaded coating on titanium implants for the prevention of implant-associated infections. Int J Nanomed 2014;9:3027.
[15] Caplin JD, Garc\'\ia AJ. Implantable antimicrobial biomaterials for local drug delivery in bone infection models. Acta Biomater 2019;93:2–11.
[16] Soleimani F, Mazaheri M, Pellerin C, Bagheri R. On the importance of noncrystalline phases in semicrystalline electrospun nanofibers. ACS Appl Polym Mater 2021;3:6315–25. https://doi.org/10.1021/acsapm.1c01088.
[17] Soleimani F, Hosseini HRM, Ordikhani F, Mokhtari-Dizaji M. Enhancing sonocatalytic properties of TiO2 nanocatalysts by controlling the surface conditions: effect of particle size and PVA modification. Desalin Water Treat 2016;57:28378–85. https://doi.org/10.1080/19443994.2016.1185746.
[18] De Tullio I, Berardini M, Di Iorio D, Perfetti F, Perfetti G. Comparative evaluation among laser-treated, machined, and sandblasted/acid-etched implant surfaces: an in vivo histologic analysis on sheep. Int J Implant Dent 2020;6:1–8.
[19] Eghbali N, Naffakh-Moosavy H, Mohammadi SS, Naderi-Manesh H. The influence of laser frequency and groove distance on cell adhesion, cell viability, and antibacterial characteristics of Ti-6Al-4V dental implants treated by modern fiber engraving laser. Dent Mater 2021;37:547–58.
[20] Raja RSS, Selvakumar P, Babu PD, Rubasingh BJ, Suresh K. Influence of laser parameters on superhydrophobicity-A review. Eng Res Express 2021;3:22001.
[21] Zhang X, Chen L. Effects of laser scanning speed on surface roughness and mechanical properties of aluminum/Polylactic Acid (Al/PLA) composites parts fabricated by fused deposition modeling. Polym Test 2020;91:106785. https://doi.org/10.1016/j.polymertesting.2020.106785.
[22] Xue X, Wu X, Liao J. Hot-cracking susceptibility and shear fracture behavior of dissimilar Ti6Al4V/AA6060 alloys in pulsed Nd:YAG laser welding. Chin J Aeronaut 2021;34:375–86. https://doi.org/10.1016/j.cja.2020.12.015.
[23] Gursel A. Crack risk in Nd: YAG laser welding of Ti-6Al-4V alloy. Mater Lett 2017;197:233–5.
[24] Chai L, Wu H, Zheng Z, Guan H, Pan H, Guo N, et al. Microstructural characterization and hardness variation of pure Ti surface-treated by pulsed laser. J Alloys Compd 2018;741:116–22.
[25] Dai J, Wang T, Chai L, Hu X, Zhang L, Guo N. Characterization and correlation of microstructure and hardness of Ti-6Al-4V sheet surface-treated by pulsed laser. J Alloys Compd 2020;826:154243.
[26] Wang T, Zeng L, Li Z, Chai L, Cheng T, Zhang L, et al. Influences of laser surface alloying with Cr on microstructural characteristics and hardness of pure Ti. Metall Mater Trans 2019;50A.

[27] Qiu Z-Y, Cui Y, Wang X-M. Natural bone tissue and its biomimetic. In: Miner. Collagen bone graft substitutes. Elsevier; 2019. p. 1–22.
[28] Braga FJC, Marques RFC, de A Filho E, Guastaldi AC. Surface modification of Ti dental implants by Nd: YVO4 laser irradiation. Appl Surf Sci 2007;253:9203–8.
[29] Wei Q, Becherer T, Angioletti-Uberti S, Dzubiella J, Wischke C, Neffe AT, et al. Protein interactions with polymer coatings and biomaterials. Angew Chem Int Ed 2014;53:8004–31.
[30] Indira K, Sylvie C, Zhongke W, Hongyu Z. Investigation of wettability properties of laser surface modified rare earth Mg alloy. Procedia Eng 2016;141:63–9.
[31] Gadelmawla ES, Koura MM, Maksoud TMA, Elewa IM, Soliman HH. Roughness parameters. J Mater Process Technol 2002;123:133–45.
[32] Chiellini E, Corti A, D'Antone S, Solaro R. Biodegradation of poly (vinyl alcohol) based materials. Prog Polym Sci 2003;28:963–1014.